

Linear Collider Signals of Z' Bosons in GUT Inspired Gauge-Higgs Unification *

Shuichiro Funatsu¹, Hisaki Hatanaka², Yutaka Hosotani³,
Yuta Orikasa⁴ and Naoki Yamatsu^{5†}

¹*Institute of Particle Physics and Key Laboratory of Quark and Lepton Physics (MOE),
Central China Normal University, Wuhan, Hubei 430079, China*

²*Osaka, Osaka 536-0014, Japan*

³*Department of Physics, Osaka University, Toyonaka, Osaka 560-0043, Japan*

⁴*Institute of Experimental and Applied Physics, Czech Technical University in Prague,
Husova 240/5, 110 00 Prague 1, Czech Republic*

⁵*Department of Physics, Kyushu University, Fukuoka 819-0395, Japan*

Abstract

In gauge-Higgs unification (GHU), the 4D Higgs boson appears as a part of the fifth dimensional component of 5D gauge field. Recently, an $SO(11)$ GUT inspired $SO(5) \times U(1) \times SU(3)$ GHU model has been proposed. In the GHU, Kaluza-Klein (KK) excited states of neutral vector bosons, photon, Z boson and Z_R boson, appear as neutral massive vector bosons Z' s. The Z' bosons in the GHU couple to quarks and leptons with large parity violation, which leads to distinctive polarization dependence in, e.g., cross sections and forward-backward asymmetries in $e^-e^+ \rightarrow \mu^-\mu^+, q\bar{q}$ processes. In the talk, we discuss fermion pair production in e^-e^+ linear collider experiments with polarized e^- and e^+ beams in the GUT inspired GHU. Deviations from the SM are shown in the early stage of planned international linear collider (ILC) with 250 GeV experiments. The deviations can be tested for the KK mass scale up to about 15 TeV. This talk is mainly based on Phys.Rev.D102(2020)015029 (Ref. [1]).

*Talk presented at the International Workshop on Future Linear Colliders (LCWS2021), 15-18 March 2021. C21-03-15.1.

†Speaker

1 Introduction

The standard model (SM), $SU(3)_C \times SU(2)_L \times U(1)_Y$ gauge theory, has been firmly established at low energies. Since the SM is not the final theory of the nature from theoretical and experimental sides, there are many attempts for constructing models beyond the SM by using many ideas such as grand unification, supersymmetry, extra-dimension, etc.

One attempt for constructing such a model is to consider gauge-Higgs unification (GHU) [2–7] in the framework of five or higher dimensional spacetime. In GHU, the Higgs field appears as a fluctuation mode of the Aharonov-Bohm (AB) phase θ_H in the extra dimension. The Higgs boson mass against quantum corrections is stabilized by the gauge symmetry. The $SU(3)_C \times SO(5) \times U(1)_X$ gauge theory in the Randall-Sundrum (RS) warped space has been proposed in Refs. [8–16]. It gives nearly the same phenomenology at low energies as the SM [11–13, 17]. For example, deviations of the gauge couplings of quarks and leptons from the SM values are less than 0.1% for $\theta_H \simeq 0.1$. Higgs couplings of quarks, leptons, W and Z bosons are approximately the SM values times $\cos \theta_H$; the deviation is about 1%.

The $SU(3)_C \times SO(5) \times U(1)_X$ GHU models predict Z' bosons, which are the Kaluza-Klein (KK) modes of γ , Z , and Z_R . In a GHU model, which is referred to as the *A-model* below, quark-lepton multiplets are introduced in the vector representation of $SO(5)$. Some results in the A-model [12, 13, 18–23] are summarized below.

- The masses of Z' bosons are in the 6 TeV–9 TeV range for $\theta_H \simeq 0.11$ –0.07, which corresponds to the KK mass scale $m_{\text{KK}} \simeq 8$ TeV–11 TeV. The current non-observation of Z' signals at 14 TeV Large Hadron Collider (LHC) puts the limit $\theta_H \lesssim 0.11$ [12, 13].
- Large parity violation appears in the couplings of quarks and leptons to KK gauge bosons, particularly to the Z' bosons. Right-handed quarks and charged leptons have rather large couplings to Z' bosons [18, 19, 21].
- Effects of KK excited neutral vector bosons, Z' bosons, on $e^-e^+ \rightarrow q\bar{q}, \ell^-\ell^+$ cross sections are studied [18, 19, 21]. In the process $e^-e^+ \rightarrow \mu^-\mu^+$, the deviation from the SM have large polarization dependence. The masses up to about 10 TeV can be explored at 250 GeV International Linear Collider (ILC) with 250 fb⁻¹ data. (For other studies, see Refs. [24–30].)

Recently, we proposed another $SU(3)_C \times SO(5) \times U(1)_X$ GHU model in Ref. [14], which is referred to as the *B-model* below. Quark-lepton multiplets are introduced in the spinor, vector, and singlet representations of $SO(5)$. The B-model can be embedded

in the $SO(11)$ gauge-Higgs grand unification [31–38], where the SM gauge group and quark-lepton content are incorporated into grand unified theory (GUT) [39–44] in higher dimensional framework [45–56].

In this talk, we mainly focus on observables in the $e^-e^+ \rightarrow \mu^-\mu^+$ process, i.e., cross section, forward-backward asymmetry [57, 58], left-right asymmetry [57–60], and left-right forward-backward asymmetry [58, 61–64]. In Ref. [1], we also studied $e^-e^+ \rightarrow f\bar{f}$ ($= c\bar{c}, b\bar{b}, t\bar{t}$) processes. (For Z' bosons in other models, see e.g., Refs. [65–67].)

The proceeding is organized as follows. In Sec. 2, the model is mention a bit. In Sec. 3, we quickly check observables such as cross section, forward-backward, left-right, and left-right forward-backward asymmetries. In Sec. 4, we describe how to detemine the parameter sets in the model. In Sec. 5, we evaluate cross sections and other observables in $e^-e^+ \rightarrow \mu^-\mu^+$ process. Section 6 is devoted to summary.

2 GUT inspired GHU (B-model)

The GUT inspired $SU(3)_C \times SO(5) \times U(1)_X$ GHU model [14] is defined in the RS warped space with metric

$$ds^2 = g_{MN}dx^M dx^N = e^{-2\sigma(y)}\eta_{\mu\nu}dx^\mu dx^\nu + dy^2, \quad (2.1)$$

where $M, N = 0, 1, 2, 3, 5$, $\mu, \nu = 0, 1, 2, 3$, $y = x^5$, $\eta_{\mu\nu} = \text{diag}(-1, +1, +1, +1)$, $\sigma(y) = \sigma(y + 2L) = \sigma(-y)$, and $\sigma(y) = ky$ for $0 \leq y \leq L$. In terms of the conformal coordinate $z = e^{ky}$ ($1 \leq z \leq z_L = e^{kL}$) in the region $0 \leq y \leq L$

$$ds^2 = \frac{1}{z^2} \left(\eta_{\mu\nu}dx^\mu dx^\nu + \frac{dz^2}{k^2} \right). \quad (2.2)$$

The bulk region $0 < y < L$ ($1 < z < z_L$) is anti-de Sitter (AdS) spacetime with a cosmological constant $\Lambda = -6k^2$, which is sandwiched by the UV brane at $y = 0$ ($z = 1$) and the IR brane at $y = L$ ($z = z_L$). The KK mass scale is $m_{\text{KK}} = \pi k / (z_L - 1) \simeq \pi k z_L^{-1}$ for $z_L \gg 1$.

Gauge fields of $SU(3)_C$, $SO(5)$, and $U(1)_X$ are denoted as $A_M^{SU(3)_C}$, $A_M^{SO(5)}$, and $A_M^{U(1)_X}$, respectively. The orbifold boundary conditions (BCs) are given by

$$\begin{pmatrix} A_\mu \\ A_y \end{pmatrix} (x, y_j - y) = P_j \begin{pmatrix} A_\mu \\ -A_y \end{pmatrix} (x, y_j + y) P_j^{-1}, \quad (y_0, y_1 = 0, L) \quad (2.3)$$

for each gauge field. $P_0 = P_1 = P_3^{SU(3)} = I_3$ for $A_M^{SU(3)_C}$ and $P_0 = P_1 = 1$ for $A_M^{U(1)_X}$. $P_0 = P_1 = P_5^{SO(5)} = \text{diag}(I_4, -I_1)$ for $A_M^{SO(5)}$ in the vector representation. The orbifold BCs $P_4^{SO(5)}$ and $P_5^{SO(5)}$ break $SO(5)$ to $SO(4) \simeq SU(2)_L \times SU(2)_R$. W , Z bosons and γ

are zero modes in the $SO(4)$ part of $A_\mu^{SO(5)}$, whereas the 4D Higgs boson is a zero mode in the $SO(5)/SO(4)$ part of $A_y^{SO(5)}$. In the GHU model, extra neutral gauge bosons Z' correspond to KK photons $\gamma^{(n)}$, KK Z bosons $Z^{(n)}$, and KK Z_R bosons $Z_R^{(n)}$ ($n \geq 1$), where the γ , and Z , Z_R bosons are the mass constants of the electro-magnetic $U(1)_{EM}$ neutral gauge bosons of $SU(2)_L$, $SU(2)_R$, and $U(1)_X$.

Matter fields in the B-model are introduced both in the 5D bulk and on the UV brane. They are listed in Table 1, which also contains the matter content in the A-model for a reference. The SM quark and lepton multiples are identified with the zero modes of the quark and lepton multiplets $\Psi_{(\mathbf{3},\mathbf{4})}^\alpha$ ($\alpha = 1, 2, 3$), $\Psi_{(\mathbf{3},\mathbf{1})}^{\pm\alpha}$, and $\Psi_{(\mathbf{1},\mathbf{4})}^\alpha$ with appropriate BCs. (For more information, see Refs. [14–16].)

	B-model			A-model	
Quark	$(\mathbf{3}, \mathbf{4})_{\frac{1}{6}}$	$(\mathbf{3}, \mathbf{1})_{-\frac{1}{3}}^+$	$(\mathbf{3}, \mathbf{1})_{-\frac{1}{3}}^-$	$(\mathbf{3}, \mathbf{5})_{\frac{2}{3}}$	$(\mathbf{3}, \mathbf{5})_{-\frac{1}{3}}$
Lepton		$(\mathbf{1}, \mathbf{4})_{-\frac{1}{2}}$		$(\mathbf{1}, \mathbf{5})_0$	$(\mathbf{1}, \mathbf{5})_{-1}$
Dark fermion	$(\mathbf{3}, \mathbf{4})_{\frac{1}{6}}$	$(\mathbf{1}, \mathbf{5})_0^+$	$(\mathbf{1}, \mathbf{5})_0^-$	$(\mathbf{1}, \mathbf{4})_{\frac{1}{2}}$	
Brane fermion		$(\mathbf{1}, \mathbf{1})_0$		$(\mathbf{3}, [\mathbf{2}, \mathbf{1}])_{\frac{7}{6}, \frac{1}{6}, -\frac{5}{6}}$ $(\mathbf{1}, [\mathbf{2}, \mathbf{1}])_{\frac{1}{2}, -\frac{1}{2}, -\frac{3}{2}}$	
Brane scalar		$(\mathbf{1}, \mathbf{4})_{\frac{1}{2}}$		$(\mathbf{1}, [\mathbf{1}, \mathbf{2}])_{\frac{1}{2}}$	

Table 1: The $SU(3)_C \times SO(5) \times U(1)_X$ content of matter fields is shown in the GUT inspired model (B-model) and the previous model (A-model).

The brane scalar field $\Phi_{(\mathbf{1},\mathbf{4})}(x)$ in $(\mathbf{1}, \mathbf{4})_{\frac{1}{2}}$ of $SU(3)_C \times SO(5) \times U(1)_X$ in Table 1 is responsible for breaking $SO(5) \times U(1)_X$ to $SU(2)_L \times U(1)_Y$. The nonvanishing vacuum expectation value (VEV) reduces the symmetry $SU(3)_C \times SO(4) \times U(1)_X$ to the SM gauge group $G_{SM} \equiv SU(3)_C \times SU(2)_L \times U(1)_Y$.

The $U(1)_Y$ gauge boson is a mixed state of $U(1)_R (\subset SU(2)_R)$ and $U(1)_X$ gauge bosons. The $U(1)_Y$ gauge field B_M^Y is given in terms of the $SU(2)_R$ gauge fields $A_M^{a_R}$ ($a_R = 1_R, 2_R, 3_R$) and the $U(1)_X$ gauge field B_M by $B_M^Y = s_\phi A_M^{3_R} + c_\phi B_M$. The mixing angle ϕ between $U(1)_R$ and $U(1)_X$ is given by $c_\phi = \cos \phi \equiv g_A / \sqrt{g_A^2 + g_B^2}$ and $s_\phi = \sin \phi \equiv g_B / \sqrt{g_A^2 + g_B^2}$ where g_A and g_B are gauge couplings in $SO(5)$ and $U(1)_X$, respectively. The 4D $SU(2)_L$ gauge coupling is given by $g_w = g_A / \sqrt{L}$. The 5D gauge coupling g_Y^{5D} of $U(1)_Y$ is given by $g_Y^{5D} = g_A g_B / \sqrt{g_A^2 + g_B^2}$. The 4D bare Weinberg angle at the tree level θ_W^0 is given by

$$\sin \theta_W^0 = \frac{s_\phi}{\sqrt{1 + s_\phi^2}}. \quad (2.4)$$

The 4D Higgs boson $\phi_H(x)$ is the zero mode in the $A_z = (kz)^{-1} A_y$ component:

$$A_z^{(j5)}(x, z) = \frac{1}{\sqrt{k}} \phi_j(x) u_H(z) + \dots, \quad u_H(z) = \sqrt{\frac{2}{z_L^2 - 1}} z, \quad \phi_H(x) = \frac{1}{\sqrt{2}} \begin{pmatrix} \phi_2 + i\phi_1 \\ \phi_4 - i\phi_3 \end{pmatrix}. \quad (2.5)$$

Without loss of generality, we assume $\langle \phi_1 \rangle, \langle \phi_2 \rangle, \langle \phi_3 \rangle = 0$ and $\langle \phi_4 \rangle \neq 0$, which is related to the AB phase θ_H in the fifth dimension by $\langle \phi_4 \rangle = \theta_H f_H$, where $f_H = (2/g_w) \sqrt{k/L(z_L^2 - 1)}$.

The gauge symmetry breaking pattern of $SU(3)_C \times SO(5) \times U(1)_X$ is given as

$$\begin{aligned}
& SU(3)_C \times SO(5) \times U(1)_X \\
& \xrightarrow{BC} SU(3)_C \times SU(2)_L \times SU(2)_R \times U(1)_X \quad \text{at } y = 0, L \\
& \xrightarrow{\langle \Phi \rangle} SU(3)_C \times SU(2)_L \times U(1)_Y \quad \text{by the VEV } \langle \Phi_{(1,4)} \rangle \neq 0 \text{ at } y = 0 \\
& \xrightarrow{\theta_H} SU(3)_C \times U(1)_{EM} \quad \text{by the Hosotani mechanism.} \tag{2.6}
\end{aligned}$$

3 Observables

We quickly check observables in $e^-e^+ \rightarrow \{V_i\} \rightarrow \mu^-\mu^+$ shown in Figure 1. Observables in $e^-e^+ \rightarrow \mu^-\mu^+$ process are summarized in Table 2. There are two observables (cross section $\sigma^{\mu^-\mu^+}$, forward-backward (FB) asymmetry $A_{FB}^{\mu^-\mu^+}$) in $e^-e^+ \rightarrow \mu^-\mu^+$ process for polarized initial state e^- and e^+ , while there are four observables (cross section $\sigma^{\mu^-\mu^+}$, forward-backward (FB) $A_{FB}^{\mu^-\mu^+}$, left-right (LR) $A_{LR}^{\mu^-\mu^+}$, LR FB asymmetries $A_{LR,FB}^{\mu^-\mu^+}$). This is because observable LR and LR FB asymmetries are zero for unpolarized initial e^- and e^+ states. (See e.g., Refs. [58, 61–64, 68].)

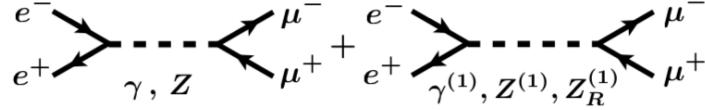


Figure 1: $e^-e^+ \rightarrow \mu^-\mu^+$ process mediated by neutral vector bosons V_i . In the SM, $V_i = \gamma, Z$. In the GHU, $V_i = \gamma, Z, \gamma^{(1)}, Z^{(1)}, Z_R^{(1)}$.

Observables	(Symbol)	Unpolarized	Polarized
Cross sections	$(\sigma^{\mu^-\mu^+})$	Yes	Yes
Forward-backward (FB) asymmetries	$(A_{FB}^{\mu^-\mu^+})$	Yes	Yes
Left-right (LR) asymmetries	$(A_{LR}^{\mu^-\mu^+})$	No	Yes
LR FB asymmetries	$(A_{LR,FB}^{\mu^-\mu^+})$	No	Yes

Table 2: Observables in $e^-e^+ \rightarrow \mu^-\mu^+$ process for unpolarized and polarized initial state e^- and e^+ . Yes/No stand for measurable/unmeasurable.

The observables in $e^-e^+ \rightarrow \mu^-\mu^+$, which are summarized in Table 3, can be expressed by four amplitudes $Q_{e_X\mu_Y}$ ($X, Y = L, R$) and an effective electron polarization P_{eff} :

$$Q_{e_X\mu_Y} = \sum_i \frac{g_{V_i e}^X g_{V_i \mu}^Y}{(s - m_{V_i}^2) + im_{V_i} \Gamma_{V_i}}, \tag{3.1}$$

where s is the square of the center-of-mass energy, $g_{V_i f}^{L/R}$ ($f = e, \mu$) are couplings of the left- and right-handed fermion f to the vector boson V_i , and m_{V_i} and Γ_{V_i} are the mass and total decay width of V_i ; the effective electron polarization is defined as

$$P_{\text{eff}} \equiv \frac{P_{e^-} - P_{e^+}}{1 - P_{e^-} P_{e^+}}. \quad (3.2)$$

where P_{e^\pm} denotes longitudinal polarization of e^\pm . $P_{e^\pm} = +1$ corresponds to purely right-handed e^\pm . (For more information, see e.g., Appendix A.)

Obs.	Linear combination of amplitudes
$\sigma^{\mu^- \mu^+}$	$(1 - P_{\text{eff}})(Q_{e_L \mu_L} ^2 + Q_{e_L \mu_R} ^2) + (1 + P_{\text{eff}})(Q_{e_R \mu_R} ^2 + Q_{e_R \mu_L} ^2)$
$A_{FB}^{\mu^- \mu^+}$	$(1 - P_{\text{eff}})(Q_{e_L \mu_L} ^2 - Q_{e_L \mu_R} ^2) + (1 + P_{\text{eff}})(Q_{e_R \mu_R} ^2 - Q_{e_R \mu_L} ^2)$
$A_{LR}^{\mu^- \mu^+}$	$ Q_{e_L \mu_L} ^2 + Q_{e_L \mu_R} ^2 - Q_{e_R \mu_R} ^2 - Q_{e_R \mu_L} ^2$
$A_{LR,FB}^{\mu^- \mu^+}$	$ Q_{e_L \mu_L} ^2 - Q_{e_L \mu_R} ^2 - Q_{e_R \mu_R} ^2 + Q_{e_R \mu_L} ^2$

Table 3: Observables ($\sigma^{\mu^- \mu^+}$, $A_{FB}^{\mu^- \mu^+}$, $A_{LR}^{\mu^- \mu^+}$, $A_{LR,FB}^{\mu^- \mu^+}$) can be expressed by linear combination of amplitudes, where overall factors are omitted and the final state muon mass is neglected.

In the following, we will show the results of $e^- e^+ \rightarrow \mu^- \mu^+$ process with polarized $e^- e^+$, $(P_{e^-}, P_{e^+}) = (\mp 0.8, \pm 0.3)$, at $\sqrt{s} = 250$ GeV with 250 fb^{-1} data in the GHU B-model. (Note that the ILC designs 80% polarization of the electron beam and 30% polarization of the positron beam according to the ILC Technical Design Report [69–73].)

In the SM, γ and Z boson contribute to the $e^- e^+ \rightarrow \mu^- \mu^+$ process. In GHU Z' bosons, $\gamma^{(n)}$, $Z^{(n)}$ and $Z_R^{(n)}$ ($n \geq 1$) give additional contributions. The masses of neutral higher KK vector bosons $Z^{(2k-1)}$, $Z^{(2k)}$, $Z_R^{(k)}$, and $\gamma^{(k)}$ ($k \geq 1$) almost linearly increase as k . The couplings constants of them to left- and right-handed electrons are decreasing when k is increasing. The contribution for the low-energy observables from each higher KK vector boson $Z^{(k)}$, $Z_R^{(k)}$, $\gamma^{(k)}$ ($k \geq 2$) is sub-dominant. In the following, we consider contributions for the low-energy observables only from the first KK bosons $Z^{(1)}$, $Z_R^{(1)}$, and $\gamma^{(1)}$.

In this talk, we focus on muon pair production, so we only list the formulas in Appendix A, which are available when the center-of-mass energy \sqrt{s} is much larger than the mass of the final state fermion m_f . We omit the non-zero final state fermion mass $m_f \neq 0$ and each statistical error estimation here. (For more information, see Ref. [1].)

4 Parameter sets

Before we calculate observables in the B-model, we need to specify parameter sets in the model. In the following, we roughly describe how to determine the parameter sets. For more information, see Ref. [1] and also Refs. [14–16].

Parameters of the model are determined in the following steps:

- (i) We pick the values of θ_H and $m_{\text{KK}} = \pi k(z_L - 1)^{-1}$.
- (ii) k is determined by reproducing the Z boson mass m_Z . The warped factor z_L is also fixed by using $m_{\text{KK}} = \pi k(z_L - 1)^{-1}$.
- (iii) The bare Weinberg angle θ_W^0 in Eq. (2.4) with given θ_H is determined to fit the observed FB asymmetry $A_{FB}^{\mu^- \mu^+} = 0.0169 \pm 0.0013$ at $\sqrt{s} = m_Z$ [74, 75].
- (iv) By using the value of $\sin \theta_W^0$, wave functions of gauge bosons are fixed.
- (v) The bulk mass parameters of quark and lepton multiplets $\Psi_{(\mathbf{3},4)}^\alpha$ and $\Psi_{(\mathbf{1},4)}^\alpha$ are fixed from the masses of up-type quarks and charged leptons.
- (vi) The bulk mass parameters of down-type quark multiplets $\Psi_{(\mathbf{3},1)}^{\pm\alpha}$ and brane interaction coefficients in the down-quark sector are determined by reproducing the masses of down-type quarks. The Majorana mass terms and brane interactions in the neutrino sector are determined by reproducing neutrino masses.

The above processes must be repeated to satisfy all the requirements for each parameter set. By using the consistent parameter sets, we proceed the following steps.

- (a) With these parameters fixed, wave functions of quarks and leptons are determined.
- (b) The Z' coupling constants to the SM fermions, etc. are determined.
- (c) The four-dimensional Z' couplings of quarks and leptons are obtained from the 5D gauge interaction terms by inserting wave functions of gauge bosons and quarks or leptons and integrating over the fifth dimensional coordinate [12, 13, 17].
- (d) By using masses and couplings of Z' bosons, decay widths of Z' bosons are calculated.

From the above procedures, we obtain some consistent parameter sets.

- The masses and widths of γ , Z boson, and the first neutral KK vector bosons $Z^{(1)}$, $Z_R^{(1)}$, $\gamma^{(1)}$ are listed in Table 4.
- The coupling constants of Z boson and the first neutral KK vector bosons $Z^{(1)}$, $Z_R^{(1)}$, $\gamma^{(1)}$ to quarks and leptons are listed in Tables 5, 6, and 7.
- Note that for $\theta_H = 0.10$ the top quark mass can be reproduced only if $z_L \geq 10^{8.1}$ and dynamical electroweak symmetry breaking is achieved only if $z_L \leq 10^{15.5}$, the values of which correspond to $m_{\text{KK}} \simeq [11, 15]$ TeV discussed in Ref. [16].

Name	θ_H [rad.]	m_{KK} [TeV]	z_L	k [GeV]	$m_{\gamma^{(1)}}$ [TeV]	$\Gamma_{\gamma^{(1)}}$ [TeV]	$m_{Z^{(1)}}$ [TeV]	$\Gamma_{Z^{(1)}}$ [TeV]	$m_{Z_R^{(1)}}$ [TeV]	$\Gamma_{Z_R^{(1)}}$ [TeV]	Table
B ^L	0.10	11.00	1.980×10^8	6.933×10^{11}	8.715	2.080	8.713	4.773	8.420	0.603	6
B	0.10	13.00	3.865×10^{11}	1.599×10^{15}	10.20	3.252	10.20	7.840	9.951	0.816	5
B ^H	0.10	15.00	2.667×10^{15}	1.273×10^{19}	11.69	4.885	11.69	11.82	11.48	1.253	7

Table 4: Masses and widths of Z' bosons ($Z^{(1)}$, $\gamma^{(1)}$, and $Z_R^{(1)}$) are listed for $\theta_H = 0.10$ and three $m_{\text{KK}} = 11, 13, 15$ TeV values. $m_Z = 91.1876$ GeV and $\Gamma_Z = 2.4952$ GeV [75]. The column “Name” denotes each parameter set and the column “Table” indicate the table summarizing coupling constants in each set. This is a part of Table III in Ref. [1].

f	g_{Zf}^L	g_{Zf}^R	$g_{Z^{(1)}f}^L$	$g_{Z^{(1)}f}^R$	$g_{Z_R^{(1)}f}^L$	$g_{Z_R^{(1)}f}^R$	$g_{\gamma^{(1)}f}^L$	$g_{\gamma^{(1)}f}^R$
e	-0.3058	0.2629	-1.7621	-0.0584	-1.0444	0	-2.7587	0.1071
μ	-0.3058	0.2629	-1.6778	-0.0584	-0.9969	0	-2.6268	0.1071

Table 5: Coupling constants of neutral vector bosons, Z' bosons, to fermions in units of $g_w = e/\sin\theta_W^0$ are listed for $\theta_H = 0.10$ and $m_{\text{KK}} = 13.00$ TeV (B) in Table 4, where $\sin^2\theta_W^0 = 0.2306$. Their corresponding Z boson coupling constants in the SM are $(g_{Z_e}^L, g_{Z_e}^R) = (-0.3065, 0.2638)$. Their corresponding γ boson coupling constants are the same as those in the SM. When the value is less than 10^{-4} , we write 0. This is a part of Table IV in Ref. [1], which contains the other coupling constants.

From Tables 5, 6, 7, we find that the coupling constants of the first neutral KK vector bosons $Z^{(1)}$, $Z_R^{(1)}$, $\gamma^{(1)}$ to quarks and leptons are larger than those of the right-handed fermions except for $Z_R^{(1)}$ couplings to the top and bottom quarks.

5 Results

In this section, we show observables of the s -channel scattering process of $e^-e^+ \rightarrow \mu^-\mu^+$ mediated by neutral vector bosons V in the GHU, where $V = \gamma, Z, \gamma^{(1)}, Z^{(1)}, Z_R^{(1)}$.

5.1 Amplitude

Cross sections are determined in terms of amplitudes $Q_{e_X\mu_Y}$ ($X, Y = L, R$) in Eq. (3.1). In Figure 2, \sqrt{s} -dependence of $s|Q_{e_X\mu_Y}|$ is displayed for the SM and GHU (B).

f	g_{Zf}^L	g_{Zf}^R	$g_{Z^{(1)}f}^L$	$g_{Z^{(1)}f}^R$	$g_{Z_R^{(1)}f}^L$	$g_{Z_R^{(1)}f}^R$	$g_{\gamma^{(1)}f}^L$	$g_{\gamma^{(1)}f}^R$
e	-0.3058	0.2629	-1.5398	-0.0695	-0.9143	0	-2.4107	0.1274
μ	-0.3058	0.2629	-1.4545	-0.0695	-0.8670	0	-2.2772	0.1274

Table 6: Coupling constants of neutral vector bosons, Z' bosons, to fermions in units of $g_w = e/\sin\theta_W^0$ are listed for $\theta_H = 0.10$ and $m_{\text{KK}} = 11.00$ TeV (B^L) in Table 4, where $\sin^2\theta_W^0 = 0.2306$. Other information is the same as in Table 5. This is a part of Table V in Ref. [1].

f	g_{Zf}^L	g_{Zf}^R	$g_{Z^{(1)}f}^L$	$g_{Z^{(1)}f}^R$	$g_{Z_R^{(1)}f}^L$	$g_{Z_R^{(1)}f}^R$	$g_{\gamma^{(1)}f}^L$	$g_{\gamma^{(1)}f}^R$
e	-0.3057	0.2629	-1.9841	-0.0504	-1.1740	0	-3.1063	0.0924
μ	-0.3057	0.2629	-1.9033	-0.0504	-1.1279	0	-2.9780	0.0924

Table 7: Coupling constants of neutral vector bosons, Z' bosons, to fermions in units of $g_w = e/\sin\theta_W^0$ are listed for $\theta_H = 0.10$ and $m_{\text{KK}} = 15.00$ TeV (B^H) in Table 4, where $\sin^2\theta_W^0 = 0.2306$. Other information is the same as in Table 5. This is a part of Table VI in Ref. [1].

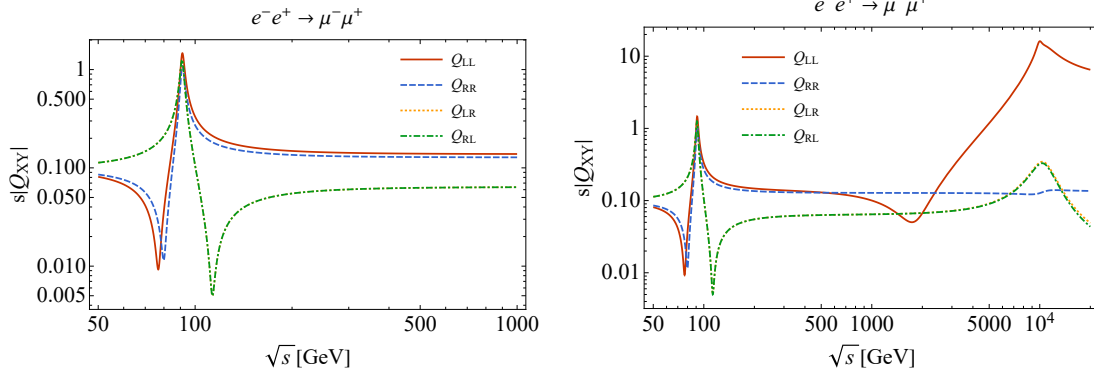


Figure 2: The amplitude $s|Q_{e_X\mu_Y}|$ ($X, Y = L, R$) vs \sqrt{s} [GeV] for the SM (left figure) and the GHU (B) (right figure) in Table 4 are shown. In each figure $Q_{e_X\mu_Y}$ is denoted as Q_{XY} . The energy ranges \sqrt{s} in the left and right figures are $\sqrt{s} = [50, 1000]$ GeV and $[50, 2 \times 10^4]$ GeV, respectively. The figures come from Figure 4 in Ref. [1].

In the SM,

$$Q_{e_X\mu_Y}^{\text{SM}} = \frac{e^2}{s} + \frac{g_{Ze}^X g_{Z\mu}^Y g_w^2}{(s - m_Z^2) + im_Z \Gamma_Z}. \quad (5.1)$$

$s|Q_{e_X\mu_Y}|$ has peak at $\sqrt{s} = m_Z$ and $Q_{e_L\mu_R} = Q_{e_R\mu_L}$. $Q_{e_L\mu_L} = Q_{e_R\mu_R}$ becomes smaller below $\sqrt{s} = m_Z$ and $Q_{e_L\mu_R}$ and $Q_{e_R\mu_L}$ become smaller above $\sqrt{s} = m_Z$ as a result of the interference of the γ and Z amplitudes. For $\sqrt{s} \gg m_Z$, $sQ_{e_X\mu_Y} \simeq e^2 + g_{Ze}^X g_{Z\mu}^Y g_w^2$. Further, the sign of the left-handed coupling constant g_{Zf}^L ($f = e, \mu$) is opposite to that of the right-handed coupling constant g_{Zf}^R , so $|Q_{e_L\mu_L}|, |Q_{e_R\mu_R}| \gg |Q_{e_L\mu_R}|, |Q_{e_R\mu_L}|$.

In GHU,

$$Q_{e_X\mu_Y} = Q_{e_X\mu_Y}^{\text{SM}} + Q_{e_X\mu_Y}^{Z'}, \quad Q_{e_X\mu_Y}^{Z'} \simeq \sum_{V=\gamma^{(1)}, Z^{(1)}, Z_R^{(1)}} \frac{g_{Ve}^X g_{V\mu}^Y g_w^2}{(s - m_V^2) + im_V \Gamma_V}, \quad (5.2)$$

where we retained contributions from first KK modes in $Q_{e_X\mu_Y}^{Z'}$. For $\sqrt{s} \lesssim 200$ GeV, $Q_{e_X\mu_Y} \sim Q_{e_X\mu_Y}^{\text{SM}}$. In Figure 2 the \sqrt{s} -dependence of $s|Q_{e_X\mu_Y}|$ is plotted. $Q_{e_X\mu_Y}$ has a peak around $\sqrt{s} \simeq m_{Z'} \simeq 10$ TeV. The dominant component is $Q_{e_L\mu_L}$, which develops significant deviation from the SM. $Q_{e_L\mu_L}$ has a dip around $\sqrt{s} \simeq 1.7$ TeV.

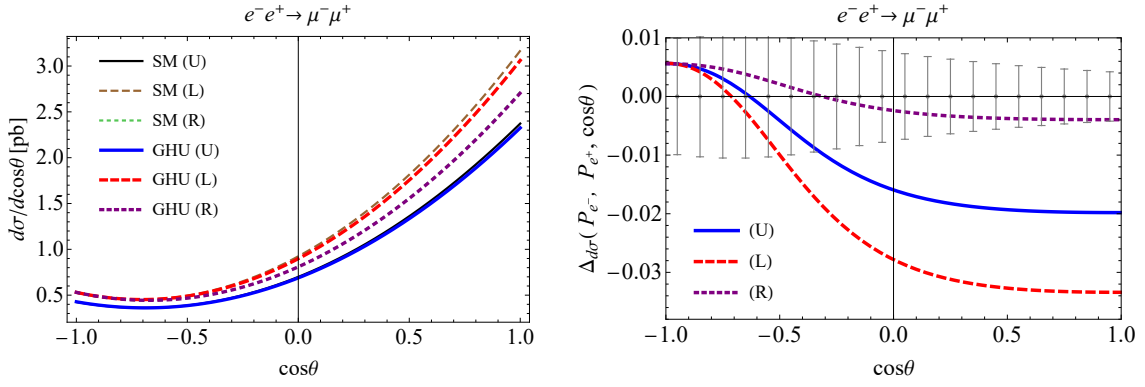


Figure 3: Differential cross section $d\sigma^{\mu^-\mu^+}/d\cos\theta$ is shown. The left figure shows the θ dependence of $d\sigma^{\mu^-\mu^+}/d\cos\theta$ in the SM and the GHU (B) in Table 4 with three sets $(P_{e^-}, P_{e^+}) = (0, 0)(U), (-0.8, +0.3)(L), (+0.8, -0.3)(R)$. $\sqrt{s} = 250$ GeV. The right figure shows the θ dependence of $\Delta_{d\sigma}^{ff}(P_{e^-}, P_{e^+}, \cos\theta)$ in Eq. (A.9). The error bars represent statistical errors in the SM at $\sqrt{s} = 250$ GeV with 250 fb^{-1} data. Each bin is given by $\cos\theta = [k - 0.05, k + 0.05]$ ($k = -0.95, -0.85, \dots, 0.95$). The figures come from Figure 5 in Ref. [1].

5.2 Cross section

The differential cross section of $e^-e^+ \rightarrow \mu^-\mu^+$ $d\sigma^{\mu^-\mu^+}/d\cos\theta$ is shown at $\sqrt{s} = 250$ GeV in Figure 3. The differential cross section in the forward region are larger than that of the backward region regardless of the polarization. The deviation from the SM are seen in the forward region with less statistical errors. The differential cross section of the 100% left- and right-handed polarized initial electron is given by the formulas in Eq. (A.3).

In the SM the Z couplings are different for left-handed and right-handed fermions which leads to $Q_{e_L\mu_L} \neq Q_{e_L\mu_R}$ and $Q_{e_R\mu_R} \neq Q_{e_R\mu_L}$.

In GHU, coupling constants of the left-handed fermions to Z' bosons are much larger than those of the right-handed ones. The magnitude of the left-handed fermion couplings is rather large so that the amount of the deviation in $d\sigma^{\mu^-\mu^+}/d\cos\theta$ from the SM becomes large for left-handed polarized electron beams, whereas the deviation becomes small for right-handed electron beams. $\Delta_{d\sigma}^{\mu^-\mu^+}(P_{e^-}, P_{e^+}, \cos\theta)$ in Eq. (A.9) is plotted in the right figure of Figure 3. The deviation for the parameter set (B) in Table 4 can be clearly seen in e^-e^+ collisions at $\sqrt{s} = 250$ GeV with 250 fb^{-1} data.

5.3 Forward-backward asymmetry

The FB asymmetry $A_{FB}^{\mu^-\mu^+}$ is shown in Figure 4. From Eq. (A.10), $A_{FB}^{\mu^-\mu^+}(P_{e^-}, P_{e^+})$ with $(P_{e^-}, P_{e^+}) = (0, 0), (-1, 0), (+1, 0)$ are given by

$$A_{FB}^{\mu^-\mu^+}(0, 0) \simeq \frac{3 \{ |Q_{e_R\mu_R}|^2 + |Q_{e_L\mu_L}|^2 \} - \{ |Q_{e_R\mu_L}|^2 + |Q_{e_L\mu_R}|^2 \}}{4 \{ |Q_{e_R\mu_R}|^2 + |Q_{e_L\mu_L}|^2 \} + \{ |Q_{e_R\mu_L}|^2 + |Q_{e_L\mu_R}|^2 \}},$$

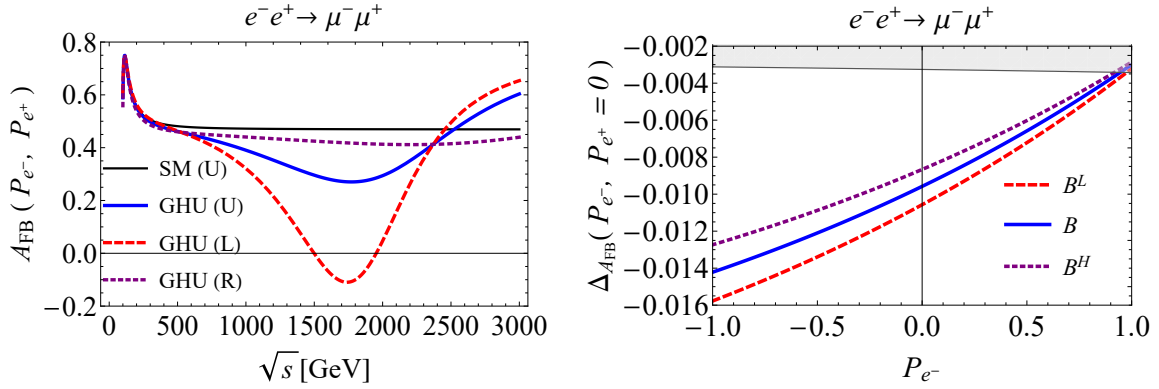


Figure 4: Forward-backward asymmetry $A_{FB}^{\mu^- \mu^+}$ is shown. The left figure shows the \sqrt{s} dependence of $A_{FB}^{f\bar{f}}$ in the SM and the GHU (B) in Table 4. Three cases of polarization of electron and positron beams $(P_{e^-}, P_{e^+}) = (0, 0)(U), (-0.8, +0.3)(L), (+0.8, -0.3)(R)$ are depicted for GHU. The energy range \sqrt{s} is [80, 3000] GeV. The right figure shows the electron polarization P_{e^-} dependence of the deviation from the SM $\Delta_{A_{FB}}^{f\bar{f}}(P_{e^-}, P_{e^+} = 0)$ in Eq. (A.12) for the GHU (B^L), (B), (B^H) in Table 4. The gray band in the central and right side figures represent the statistical error in the SM at $\sqrt{s} = 250$ GeV with 250 fb^{-1} data. The figures come from Figure 6 in Ref. [1].

$$\begin{aligned}
A_{FB}^{\mu^- \mu^+}(-1, 0) &\simeq \frac{3}{4} \frac{|Q_{e_L \mu_L}|^2 - |Q_{e_L \mu_R}|^2}{|Q_{e_L \mu_L}|^2 + |Q_{e_L \mu_R}|^2}, \\
A_{FB}^{\mu^- \mu^+}(1, 0) &\simeq \frac{3}{4} \frac{|Q_{e_R \mu_R}|^2 - |Q_{e_R \mu_L}|^2}{|Q_{e_R \mu_R}|^2 + |Q_{e_R \mu_L}|^2}.
\end{aligned} \tag{5.3}$$

In the SM, the FB asymmetry $A_{FB}^{\mu^- \mu^+}$ becomes constant for $\sqrt{s} \gg m_Z$. $A_{FB}^{\mu^- \mu^+}(P_{e^-}, P_{e^+})$ becomes small at Z -pole $\sqrt{s} = m_Z$. $A_{FB}^{\mu^- \mu^+}(P_{e^-}, P_{e^+}) \simeq 3/4$ slightly above Z -pole $\sqrt{s} = m_Z$. $A_{FB}^{\mu^- \mu^+}(P_{e^-}, P_{e^+})$ approaches constant for $\sqrt{s} \gg m_Z$.

In the GHU (B) in Table 4, due to the interference effects among Z and Z' bosons, $|Q_{e_L \mu_L}|$ can be smaller than $|Q_{e_L \mu_R}|$ in some energy region (around $\sqrt{s} \sim 1.7 \text{ TeV}$). Consequently $A_{FB}^{\mu^- \mu^+}$ can become negative even for $\sqrt{s} \gg m_Z$ as shown in Figure 4. Deviation from the SM starts to show up around $\sqrt{s} = 250$ GeV. As shown in the right figure in Figure 4, the amount of the deviation $\Delta_{A_{FB}}^{\mu^- \mu^+}(P_{e^-}, P_{e^+} = 0)$ in Eq. (A.12) becomes significant for $P_{e^-} \sim -1$ even at $\sqrt{s} = 250$ GeV.

5.4 Left-right asymmetry

The LR asymmetry $A_{LR}^{\mu^- \mu^+}(\cos \theta)$ is given by Eq. (A.14), and is displayed in Figure 5. In most of center-of-mass energy region of interest, relations $|Q_{e_L \mu_L}| \gg |Q_{e_L \mu_R}|$ and $|Q_{e_R \mu_R}| \gg |Q_{e_R \mu_L}|$ are satisfied so that in the forward region $\cos \theta > 0$, the LR asymmetry is approximately

$$A_{LR}^{f\bar{f}}(\cos \theta) \simeq \frac{|Q_{e_L \mu_L}|^2 - |Q_{e_R \mu_R}|^2}{|Q_{e_L \mu_L}|^2 + |Q_{e_R \mu_R}|^2}. \tag{5.4}$$

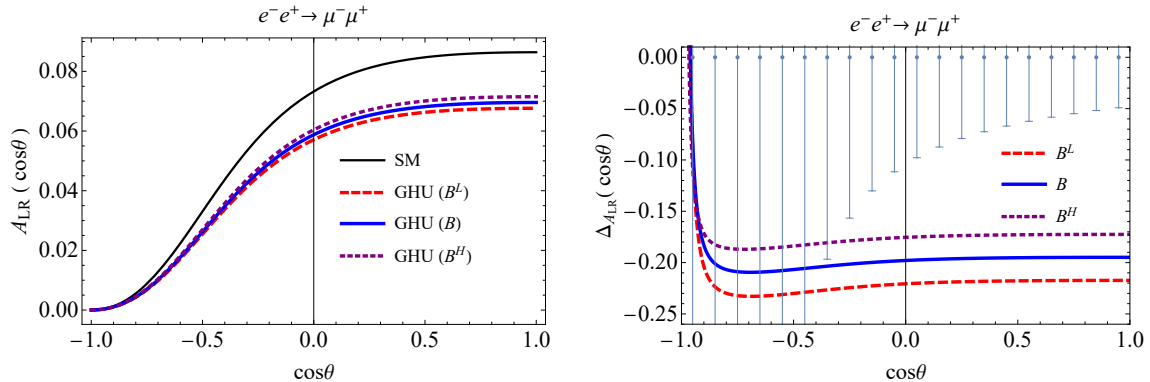


Figure 5: Left-right asymmetry $A_{LR}^{\mu^- \mu^+}(\cos \theta)$ is shown. The left figure shows the θ dependence of $A_{LR}^{\mu^- \mu^+}(\cos \theta)$ for the SM and the GHU (B^L), (B), (B^H) in Table 4. The right figure shows the θ dependence of the deviation of the left-right asymmetry from the SM, $\Delta_{A_{LR}}^{\mu^- \mu^+}(\cos \theta)$ in Eq. (A.21) for the GHU (B^L), (B), (B^H). The error bars in the right side figures represent the statistical error at $\sqrt{s} = 250$ GeV with 250 fb^{-1} data and $(P_{e^-}, P_{e^+}) = (-0.8, +0.3), (+0.8, -0.3)$. The figures come from Figure 8 in Ref. [1].

5.5 Left-right forward-backward asymmetry

The LR FB asymmetry $A_{LR,FB}^{\mu^- \mu^+}(\cos \theta)$ is given by in Eq. (A.23). It is shown in Figure 6. For $|Q_{e_L \mu_L}| \gg |Q_{e_L \mu_R}|$, $|Q_{e_R \mu_R}| \gg |Q_{e_R \mu_L}|$, the LR FB asymmetry can be written in terms of the integrated LR asymmetry $A_{LR}^{\mu^- \mu^+}$ by

$$A_{LR,FB}^{\mu^- \mu^+}(\cos \theta) \simeq \frac{2 \cos \theta}{1 + \cos^2 \theta} \frac{|Q_{e_L \mu_L}|^2 - |Q_{e_R \mu_R}|^2}{|Q_{e_L \mu_L}|^2 + |Q_{e_R \mu_R}|^2} \simeq \frac{2 \cos \theta}{1 + \cos^2 \theta} A_{LR}^{\mu^- \mu^+}. \quad (5.5)$$

6 Summary

We showed some results for cross sections, forward-backward (FB), left-right (LR), and left-right forward-backward (LR FB) asymmetries in the process $e^- e^+ \rightarrow \mu^- \mu^+$ in the GUT inspired GHU model (B-model). Clear deviations from the SM should be observed in the early stage of ILC 250 GeV experiments. In particular, GHU predicts strong dependence on the polarization of e^- and e^+ beams, with which one can explore physics at the KK mass scale of 15 TeV.

In the talk, we focused on the analysis of the s -channel scattering processes $e^- e^+ \rightarrow \mu^- \mu^+$ mediated by neutral vector bosons Z' in the GHU B-model. For $e^- e^+ \rightarrow e^- e^+$, there is a contribution not only from the s -channel scattering process but also from the t -channel scattering process [25, 68, 76–79]. It has been pointed out in Ref. [25] that for the scattering process $e^- e^+ \rightarrow e^- e^+$, deviations from the SM in the GHU A-model can be detected even in the early stage of the ILC experiment at 250 GeV. Therefore we also expect similar deviations from the SM in the GHU B-model. We are now preparing for a paper about the $e^- e^+ \rightarrow e^- e^+$ scattering process in GHU, which will appear soon.

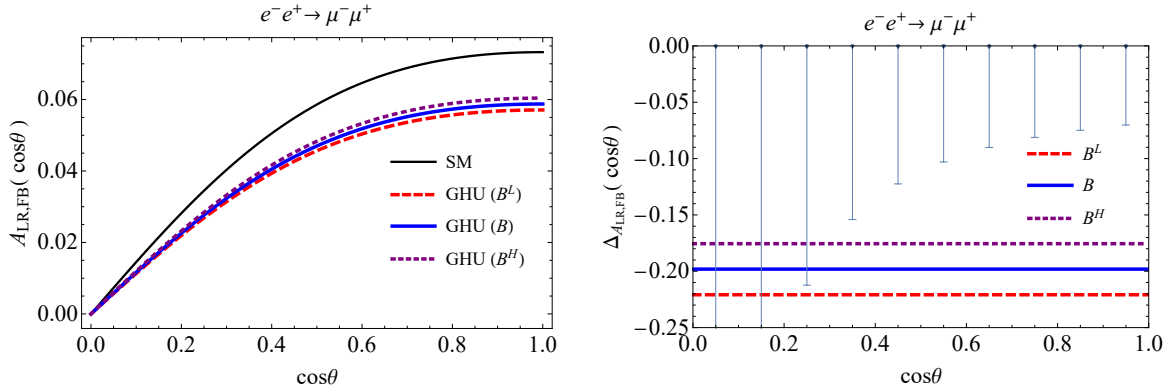


Figure 6: Left-right forward-backward asymmetry $A_{LR,FB}^{\mu^-\mu^+}(\cos\theta)$ is shown. The left figure shows the \sqrt{s} dependence of $A_{LR,FB}^{\mu^-\mu^+}(\cos\theta)$ for the SM and the GHU (B^L), (B), (B^H) in Table 4. The right figure shows the $\cos\theta$ dependence of the deviation of the left-right asymmetry from the SM, $\Delta_{A_{LR,FB}}(\cos\theta)$ in Eq. (A.26) for the GHU (B^L), (B), (B^H) in Table 4. The error bars in the right side figures stand for the statistical error at $\sqrt{s} = 250$ GeV with 250fb^{-1} data and $(P_{e^-}, P_{e^+}) = (-0.8, +0.3), (+0.8, -0.3)$. The figures come from Figure 9 in Ref. [1].

Acknowledgments

This work was supported in part by European Regional Development Fund-Project Engineering Applications of Microworld Physics (No. CZ.02.1.01/0.0/0.0/16_019/0000766) (Y.O.), by the National Natural Science Foundation of China (Grant Nos. 11775092, 11675061, 11521064, 11435003 and 11947213) (S.F.), by the International Postdoctoral Exchange Fellowship Program (IPEFP) (S.F.), and by Japan Society for the Promotion of Science, Grants-in-Aid for Scientific Research, No. JP19K03873 (Y.H.) and Nos. JP18H05543 and JP19K23440 (N.Y.).

A Observables

Here we summarize formulas of several observables in the s -channel scattering processes of $e^-e^+ \rightarrow f\bar{f}$ mediated by only neutral vector bosons V_i . In the proceeding, we consider $f\bar{f} = \mu^-\mu^+$, so we neglect the final state fermion mass. The formulas with nonzero fermion mass are give in e.g., Ref. [1]. For more information, see Ref. [1] and the references.

A.1 Cross section

The differential cross section for the $e^-e^+ \rightarrow f\bar{f}$ process is given by

$$\begin{aligned} & \frac{d\sigma^{f\bar{f}}}{d\cos\theta}(P_{e^-}, P_{e^+}, \cos\theta) \\ &= (1 - P_{e^-}P_{e^+}) \frac{1}{4} \left\{ (1 - P_{\text{eff}}) \frac{d\sigma_{LR}^{f\bar{f}}}{d\cos\theta}(\cos\theta) + (1 + P_{\text{eff}}) \frac{d\sigma_{RL}^{f\bar{f}}}{d\cos\theta}(\cos\theta) \right\} \quad (\text{A.1}) \end{aligned}$$

where P_{e^\pm} denotes longitudinal polarization of e^\pm . $P_{e^\pm} = +1$ corresponds to purely right-handed e^\pm . P_{eff} is defined as

$$P_{\text{eff}} \equiv \frac{P_{e^-} - P_{e^+}}{1 - P_{e^-} P_{e^+}}. \quad (\text{A.2})$$

$d\sigma_{LR}/d\cos\theta$ and $d\sigma_{RL}/d\cos\theta$ are differential cross sections for $e_L^- e_R^+ \rightarrow f\bar{f}$ and $e_R^- e_L^+ \rightarrow f\bar{f}$:

$$\begin{aligned} \frac{d\sigma_{LR}^{f\bar{f}}}{d\cos\theta}(\cos\theta) &\simeq \frac{s}{32\pi} \left\{ (1 + \cos\theta)^2 |Q_{e_L f_L}|^2 + (1 - \cos\theta)^2 |Q_{e_L f_R}|^2 \right\}, \\ \frac{d\sigma_{RL}^{f\bar{f}}}{d\cos\theta}(\cos\theta) &\simeq \frac{s}{32\pi} \left\{ (1 + \cos\theta)^2 |Q_{e_R f_R}|^2 + (1 - \cos\theta)^2 |Q_{e_R f_L}|^2 \right\}. \end{aligned} \quad (\text{A.3})$$

$Q_{e_X f_Y}$ ($X, Y = L, R$) are given by

$$Q_{e_X f_Y} \equiv \sum_i \frac{g_{V_i e}^X g_{V_i f}^Y}{(s - m_{V_i}^2) + im_{V_i} \Gamma_{V_i}}, \quad (\text{A.4})$$

where $g_{V_i f}^{L/R}$ are couplings of the left- and right-handed fermion f to the vector boson V_i , and m_{V_i} and Γ_{V_i} are the mass and total decay width of V_i .

The differential cross section integrated over the angle $\theta = [\theta_1, \theta_2]$ is given by

$$\sigma^{f\bar{f}}(P_{e^-}, P_{e^+}, [\cos\theta_1, \cos\theta_2]) \equiv \int_{\cos\theta_1}^{\cos\theta_2} \frac{d\sigma^{f\bar{f}}}{d\cos\theta}(P_{e^-}, P_{e^+}, \cos\theta) d\cos\theta, \quad (\text{A.5})$$

where $\frac{d\sigma^{f\bar{f}}}{d\cos\theta}(P_{e^-}, P_{e^+}, \cos\theta)$ is given in Eq. (A.1). The observed total cross section $\sigma_{\text{tot}}^{f\bar{f}}(P_{e^-}, P_{e^+})$ is given by

$$\sigma_{\text{tot}}^{f\bar{f}}(P_{e^-}, P_{e^+}) = \sigma^{f\bar{f}}(P_{e^-}, P_{e^+}, [-\cos\theta_{\text{max}}, +\cos\theta_{\text{max}}]), \quad (\text{A.6})$$

where the available value of θ_{max} depends on each experiment. The cross section $\sigma_{\text{tot}}^{f\bar{f}}(P_{e^-}, P_{e^+})$ is given by

$$\sigma_{\text{tot}}^{f\bar{f}}(P_{e^-}, P_{e^+}) = (1 - P_{e^-} P_{e^+}) \cdot \frac{1}{4} \left\{ (1 - P_{\text{eff}}) \sigma_{LR}^{f\bar{f}} + (1 + P_{\text{eff}}) \sigma_{RL}^{f\bar{f}} \right\}, \quad (\text{A.7})$$

where for the available value of $\theta_{\text{max}} = 1$,

$$\sigma_{LR}^{f\bar{f}} \simeq \frac{s}{12\pi} (|Q_{e_L f_L}|^2 + |Q_{e_L f_R}|^2), \quad \sigma_{RL}^{f\bar{f}} \simeq \frac{s}{12\pi} (|Q_{e_R f_R}|^2 + |Q_{e_R f_L}|^2). \quad (\text{A.8})$$

The amount of the deviation from the SM in the differential cross section for $e^- e^+ \rightarrow f\bar{f}$ is characterized by

$$\Delta_{d\sigma}^{f\bar{f}}(P_{e^-}, P_{e^+}, \cos\theta) \equiv \frac{\frac{d\sigma_{\text{GHU}}^{f\bar{f}}}{d\cos\theta}(P_{e^-}, P_{e^+}, \cos\theta)}{\frac{d\sigma_{\text{SM}}^{f\bar{f}}}{d\cos\theta}(P_{e^-}, P_{e^+}, \cos\theta)} - 1. \quad (\text{A.9})$$

A.2 Forward-backward asymmetry

The forward-backward asymmetry $A_{FB}^{f\bar{f}}(P_{e^-}, P_{e^+})$ [57, 58] is given by

$$\begin{aligned} A_{FB}^{f\bar{f}}(P_{e^-}, P_{e^+}) &= \frac{\sigma_F^{f\bar{f}}(P_{e^-}, P_{e^+}) - \sigma_B^{f\bar{f}}(P_{e^-}, P_{e^+})}{\sigma_F^{f\bar{f}}(P_{e^-}, P_{e^+}) + \sigma_B^{f\bar{f}}(P_{e^-}, P_{e^+})}, \\ \sigma_F^{f\bar{f}}(P_{e^-}, P_{e^+}) &= \sigma^{f\bar{f}}(P_{e^-}, P_{e^+}, [0, +\cos\theta_{\max}]), \\ \sigma_B^{f\bar{f}}(P_{e^-}, P_{e^+}) &= \sigma^{f\bar{f}}(P_{e^-}, P_{e^+}, [-\cos\theta_{\max}, 0]), \end{aligned} \quad (\text{A.10})$$

By using $Q_{e_X f_Y}(X, Y = L, R)$ in Eq. (A.4), for $\cos\theta_{\max} = 1$,

$$\begin{aligned} A_{FB}^{f\bar{f}}(P_{e^-}, P_{e^+}) &\simeq \frac{3B_1 - B_2}{4B_1 + B_2}, \\ B_1 &= (1 + P_{\text{eff}})|Q_{e_R f_R}|^2 + (1 - P_{\text{eff}})|Q_{e_L f_L}|^2, \\ B_2 &= (1 + P_{\text{eff}})|Q_{e_R f_L}|^2 + (1 - P_{\text{eff}})|Q_{e_L f_R}|^2, \end{aligned} \quad (\text{A.11})$$

where P_{eff} is given in Eq. (A.2).

The amount of the deviation from the SM is characterized by

$$\Delta_{AFB}^{f\bar{f}} \equiv \frac{A_{FB, \text{GHU}}^{f\bar{f}}}{A_{FB, \text{SM}}^{f\bar{f}}} - 1. \quad (\text{A.12})$$

A.3 Left-right asymmetry

The left-right asymmetry [57, 58, 68] is given by

$$A_{LR}^{f\bar{f}}(\cos\theta) = \frac{\sigma_{LR}^{f\bar{f}}(\cos\theta) - \sigma_{RL}^{f\bar{f}}(\cos\theta)}{\sigma_{LR}^{f\bar{f}}(\cos\theta) + \sigma_{RL}^{f\bar{f}}(\cos\theta)}, \quad (\text{A.13})$$

where $\sigma_{LR}^{f\bar{f}}(\cos\theta)$ and $\sigma_{RL}^{f\bar{f}}(\cos\theta)$ stand for $\frac{d\sigma_{LR}^{f\bar{f}}}{d\cos\theta}(\cos\theta)$ and $\frac{d\sigma_{RL}^{f\bar{f}}}{d\cos\theta}(\cos\theta)$ in Eq. (A.3), respectively.

$$A_{LR}^{f\bar{f}}(\cos\theta) \simeq \frac{(1 + \cos\theta)^2 (|Q_{e_L f_L}|^2 - |Q_{e_R f_R}|^2) + (1 - \cos\theta)^2 (|Q_{e_L f_R}|^2 - |Q_{e_R f_L}|^2)}{(1 + \cos\theta)^2 (|Q_{e_L f_L}|^2 + |Q_{e_R f_R}|^2) + (1 - \cos\theta)^2 (|Q_{e_L f_R}|^2 + |Q_{e_R f_L}|^2)}. \quad (\text{A.14})$$

The observable left-right asymmetry is given by

$$A_{LR}^{f\bar{f}}(P_{e^-}, P_{e^+}, \cos\theta) = \frac{\sigma^{f\bar{f}}(P_{e^-}, P_{e^+}, \cos\theta) - \sigma^{f\bar{f}}(-P_{e^-}, -P_{e^+}, \cos\theta)}{\sigma^{f\bar{f}}(P_{e^-}, P_{e^+}, \cos\theta) + \sigma^{f\bar{f}}(-P_{e^-}, -P_{e^+}, \cos\theta)} \quad (\text{A.15})$$

for $P_{e^-} < 0$ and $|P_{e^-}| > |P_{e^+}|$, where $\sigma^{f\bar{f}}(P_{e^-}, P_{e^+}, \cos\theta)$ and $\sigma^{f\bar{f}}(-P_{e^-}, -P_{e^+}, \cos\theta)$ stand for $\frac{d\sigma^{f\bar{f}}}{d\cos\theta}(P_{e^-}, P_{e^+}, \cos\theta)$ and $\frac{d\sigma^{f\bar{f}}}{d\cos\theta}(-P_{e^-}, -P_{e^+}, \cos\theta)$ in Eq. (A.1), respectively. (A.15) is related to (A.13) by

$$A_{LR}^{f\bar{f}}(\cos\theta) = \frac{1}{P_{\text{eff}}} A_{LR}^{f\bar{f}}(P_{e^-}, P_{e^+}, \cos\theta). \quad (\text{A.16})$$

The integrated left-right asymmetry $A_{LR}^{f\bar{f}}$ [57, 58] is given by

$$A_{LR}^{f\bar{f}} = \frac{\sigma_{LR}^{f\bar{f}} - \sigma_{RL}^{f\bar{f}}}{\sigma_{LR}^{f\bar{f}} + \sigma_{RL}^{f\bar{f}}}. \quad (\text{A.17})$$

By using $Q_{exf_Y}(X, Y = L, R)$ in Eq. (A.4), $A_{LR}^{f\bar{f}}$ is expressed as

$$A_{LR}^{f\bar{f}} \simeq \frac{[|Q_{eLfL}|^2 + |Q_{eLfR}|^2] - [|Q_{eRfR}|^2 + |Q_{eRfL}|^2]}{[|Q_{eLfL}|^2 + |Q_{eLfR}|^2] + [|Q_{eRfR}|^2 + |Q_{eRfL}|^2]}. \quad (\text{A.18})$$

The observable left-right asymmetry is given by

$$A_{LR}^{f\bar{f}}(P_{e^-}, P_{e^+}) = \frac{\sigma^{f\bar{f}}(P_{e^-}, P_{e^+}) - \sigma^{f\bar{f}}(-P_{e^-}, -P_{e^+})}{\sigma^{f\bar{f}}(P_{e^-}, P_{e^+}) + \sigma^{f\bar{f}}(-P_{e^-}, -P_{e^+})} \quad (\text{A.19})$$

for $P_{e^-} < 0$ and $|P_{e^-}| > |P_{e^+}|$. It is related to (A.17) by

$$A_{LR}^{f\bar{f}} = \frac{1}{P_{\text{eff}}} A_{LR}^{f\bar{f}}(P_{e^-}, P_{e^+}). \quad (\text{A.20})$$

The amount of the deviation from the SM in (A.16) and (A.17) is characterized by

$$\begin{aligned} \Delta_{ALR}^{f\bar{f}}(\cos\theta) &\equiv \frac{A_{LR,\text{GHU}}^{f\bar{f}}(\cos\theta)}{A_{LR,\text{SM}}^{f\bar{f}}(\cos\theta)} - 1, \\ \Delta_{ALR}^{f\bar{f}} &\equiv \frac{A_{LR,\text{GHU}}^{f\bar{f}}}{A_{LR,\text{SM}}^{f\bar{f}}} - 1. \end{aligned} \quad (\text{A.21})$$

A.4 Left-right forward-backward asymmetry

The left-right forward-backward asymmetry [58, 61–64] is given by

$$A_{LR,FB}^{f\bar{f}}(\cos\theta) = \frac{[\sigma_{LR}^{f\bar{f}}(\cos\theta) - \sigma_{RL}^{f\bar{f}}(\cos\theta)] - [\sigma_{LR}^{f\bar{f}}(-\cos\theta) - \sigma_{RL}^{f\bar{f}}(-\cos\theta)]}{[\sigma_{LR}^{f\bar{f}}(\cos\theta) + \sigma_{RL}^{f\bar{f}}(\cos\theta)] + [\sigma_{LR}^{f\bar{f}}(-\cos\theta) + \sigma_{RL}^{f\bar{f}}(-\cos\theta)]}. \quad (\text{A.22})$$

In terms of $Q_{exf_Y}(X, Y = L, R)$ in Eq. (A.4), $A_{LR,FB}^{f\bar{f}}$ is expressed as

$$\begin{aligned} A_{LR,FB}^{f\bar{f}}(\cos\theta) &\simeq \frac{2 \cos\theta}{1 + \cos^2\theta} \frac{D_-}{D_+}, \\ D_{\pm} &= (|Q_{eLfL}|^2 + |Q_{eRfL}|^2) \pm (|Q_{eLfR}|^2 + |Q_{eRfR}|^2). \end{aligned} \quad (\text{A.23})$$

The observable left-right forward-backward asymmetry is given by

$$\begin{aligned} A_{LR,FB}^{f\bar{f}}(P_{e^-}, P_{e^+}, \cos\theta) &= \frac{E_-}{E_+}, \\ E_{\pm} &= [\sigma^{f\bar{f}}(P_{e^-}, P_{e^+}, \cos\theta) + \sigma^{f\bar{f}}(-P_{e^-}, -P_{e^+}, -\cos\theta)] \\ &\quad \pm [\sigma^{f\bar{f}}(-P_{e^-}, -P_{e^+}, \cos\theta) + \sigma^{f\bar{f}}(P_{e^-}, P_{e^+}, -\cos\theta)] \end{aligned} \quad (\text{A.24})$$

for $P_{e^-} < 0$ and $|P_{e^-}| > |P_{e^+}|$. The relation between $A_{LR,FB}^{f\bar{f}}(\cos\theta)$ in Eq. (A.22) and $A_{LR,FB}^{f\bar{f}}(P_{e^-}, P_{e^+}, \cos\theta)$ in Eq. (A.24) is given by

$$A_{LR,FB}^{f\bar{f}}(\cos\theta) = \frac{1}{P_{\text{eff}}} A_{LR,FB}^{f\bar{f}}(P_{e^-}, P_{e^+}, \cos\theta) . \quad (\text{A.25})$$

The amount of the deviation in $A_{LR,FB}$ from the SM is characterized by

$$\Delta_{A_{LR,FB}}^{f\bar{f}}(\cos\theta) \equiv \frac{A_{LR,FB,\text{GHU}}^{f\bar{f}}(\cos\theta)}{A_{LR,FB,\text{SM}}^{f\bar{f}}(\cos\theta)} - 1 . \quad (\text{A.26})$$

References

- [1] S. Funatsu, H. Hatanaka, Y. Hosotani, Y. Orikasa, and N. Yamatsu, ‘‘Fermion Pair Production at e^-e^+ Linear Collider Experiments in GUT Inspired Gauge-Higgs Unification,’’ *Phys. Rev. D* **102** (2020) 015029, [arXiv:2006.02157 \[hep-ph\]](#).
- [2] Y. Hosotani, ‘‘Dynamical Mass Generation by Compact Extra Dimensions,’’ *Phys.Lett.* **B126** (1983) 309.
- [3] Y. Hosotani, ‘‘Dynamics of Nonintegrable Phases and Gauge Symmetry Breaking,’’ *Annals Phys.* **190** (1989) 233.
- [4] A. T. Davies and A. McLachlan, ‘‘Gauge Group Breaking By Wilson Loops,’’ *Phys. Lett.* **B200** (1988) 305.
- [5] A. T. Davies and A. McLachlan, ‘‘Congruency Class Effects in the Hosotani Model,’’ *Nucl. Phys.* **B317** (1989) 237.
- [6] H. Hatanaka, T. Inami, and C. S. Lim, ‘‘The Gauge Hierarchy Problem and Higher Dimensional Gauge Theories,’’ *Mod. Phys. Lett.* **A13** (1998) 2601–2612, [arXiv:hep-th/9805067](#).
- [7] H. Hatanaka, ‘‘Matter Representations and Gauge Symmetry Breaking via Compactified Space,’’ *Prog. Theor. Phys.* **102** (1999) 407–418, [arXiv:hep-th/9905100 \[hep-th\]](#).
- [8] K. Agashe, R. Contino, and A. Pomarol, ‘‘The Minimal Composite Higgs Model,’’ *Nucl. Phys.* **B719** (2005) 165–187, [arXiv:hep-ph/0412089 \[hep-ph\]](#).
- [9] A. D. Medina, N. R. Shah, and C. E. M. Wagner, ‘‘Gauge-Higgs Unification and Radiative Electroweak Symmetry Breaking in Warped Extra Dimensions,’’ *Phys. Rev.* **D76** (2007) 095010, [arXiv:0706.1281 \[hep-ph\]](#).
- [10] Y. Hosotani, K. Oda, T. Ohnuma, and Y. Sakamura, ‘‘Dynamical Electroweak Symmetry Breaking in $SO(5) \times U(1)$ Gauge-Higgs Unification with Top and Bottom Quarks,’’ *Phys.Rev.* **D78** (2008) 096002, [arXiv:0806.0480 \[hep-ph\]](#).
- [11] S. Funatsu, H. Hatanaka, Y. Hosotani, Y. Orikasa, and T. Shimotani, ‘‘Novel Universality and Higgs Decay $H \rightarrow \gamma\gamma$, gg in the $SO(5) \times U(1)$ Gauge-Higgs Unification,’’ *Phys. Lett.* **B722** (2013) 94–99, [arXiv:1301.1744 \[hep-ph\]](#).
- [12] S. Funatsu, H. Hatanaka, Y. Hosotani, Y. Orikasa, and T. Shimotani, ‘‘LHC Signals of the $SO(5) \times U(1)$ Gauge-Higgs Unification,’’ *Phys. Rev.* **D89** no. 9, (2014) 095019, [arXiv:1404.2748 \[hep-ph\]](#).

- [13] S. Funatsu, H. Hatanaka, Y. Hosotani, and Y. Orikasa, “Collider Signals of W' and Z' Bosons in the Gauge-Higgs Unification,” *Phys. Rev. D* **95** no. 3, (2017) 035032, [arXiv:1612.03378 \[hep-ph\]](#).
- [14] S. Funatsu, H. Hatanaka, Y. Hosotani, Y. Orikasa, and N. Yamatsu, “GUT Inspired $SO(5) \times U(1) \times SU(3)$ Gauge-Higgs Unification,” *Phys. Rev. D* **99** (2019) 095010, [arXiv:1902.01603 \[hep-ph\]](#).
- [15] S. Funatsu, H. Hatanaka, Y. Hosotani, Y. Orikasa, and N. Yamatsu, “CKM Matrix and FCNC Suppression in $SO(5) \times U(1) \times SU(3)$ Gauge-Higgs Unification,” *Phys. Rev. D* **101** (2020) 055016, [arXiv:1909.00190 \[hep-ph\]](#).
- [16] S. Funatsu, H. Hatanaka, Y. Hosotani, Y. Orikasa, and N. Yamatsu, “Effective Potential and Universality in GUT-Inspired Gauge-Higgs Unification,” *Phys. Rev. D* **102** (2020) 015005, [arXiv:2002.09262 \[hep-ph\]](#).
- [17] S. Funatsu, H. Hatanaka, and Y. Hosotani, “ $H \rightarrow Z\gamma$ in the Gauge-Higgs Unification,” *Phys. Rev.* **D92** (2015) 115003, [arXiv:1510.06550 \[hep-ph\]](#).
- [18] S. Funatsu, H. Hatanaka, Y. Hosotani, and Y. Orikasa, “Distinct Signals of the Gauge-Higgs Unification in e^+e^- Collider Experiments,” *Phys. Lett.* **B775** (2017) 297–302, [arXiv:1705.05282 \[hep-ph\]](#).
- [19] J. Yoon and M. E. Peskin, “Fermion Pair Production in $SO(5) \times U(1)$ Gauge-Higgs Unification Models,” [arXiv:1811.07877 \[hep-ph\]](#).
- [20] J. Yoon and M. E. Peskin, “Dissection of an $SO(5) \times U(1)$ Gauge-Higgs Unification Model,” *Phys. Rev.* **D100** no. 1, (2019) 015001, [arXiv:1810.12352 \[hep-ph\]](#).
- [21] S. Funatsu, “Forward-Backward Asymmetry in the Gauge-Higgs Unification at the International Linear Collider,” *Eur. Phys. J.* **C79** no. 10, (2019) 854, [arXiv:1905.10007 \[hep-ph\]](#).
- [22] Y. Hosotani, “Gauge-Higgs Unification at e^+e^- Linear Colliders,” *PoS CORFU2018* (2019) 075, [arXiv:1904.10156 \[hep-ph\]](#).
- [23] S. Funatsu, “Forward-Backward Asymmetry in the Gauge-Higgs Unification at the International Linear Collider,” *PoS CORFU2019* (2020) 088.
- [24] S. Bilokin, R. Pöschl, and F. Richard, “Measurement of b Quark EW Couplings at ILC,” [arXiv:1709.04289 \[hep-ex\]](#).
- [25] F. Richard, “Bhabha Scattering at ILC250,” [arXiv:1804.02846 \[hep-ex\]](#).
- [26] A. Irlles, R. Pöschl, F. Richard, and H. Yamamoto, “Complementarity between ILC250 and ILC-GigaZ,” in *Linear Collider Community Meeting Lausanne, Switzerland. 2019.* [arXiv:1905.00220 \[hep-ex\]](#).
- [27] A. Irlles, R. Pöschl, and F. Richard, “Production and Measurement of $e^+e^- \rightarrow c\bar{c}$ Signatures at the 250 GeV ILC,” in *International Workshop on Future Linear Colliders (LCWS 2019), Japan. 2019.* [arXiv:2002.05805 \[hep-ex\]](#).
- [28] K. Fujii et al., “Physics Case for the 250 GeV Stage of the International Linear Collider,” [arXiv:1710.07621 \[hep-ex\]](#).
- [29] **ILC** Collaboration, H. Aihara et al., “The International Linear Collider. A Global Project,” [arXiv:1901.09829 \[hep-ex\]](#).

- [30] P. Bambade et al., “The International Linear Collider: A Global Project,” [arXiv:1903.01629](#) [hep-ex].
- [31] Y. Hosotani and N. Yamatsu, “Gauge-Higgs Grand Unification,” *Prog. Theor. Exp. Phys.* **2015** (2015) 111B01, [arXiv:1504.03817](#) [hep-ph].
- [32] N. Yamatsu, “Gauge Coupling Unification in Gauge-Higgs Grand Unification,” *Prog. Theor. Exp. Phys.* **2016** (2016) 043B02, [arXiv:1512.05559](#) [hep-ph].
- [33] A. Furui, Y. Hosotani, and N. Yamatsu, “Toward Realistic Gauge-Higgs Grand Unification,” *Prog. Theor. Exp. Phys.* **2016** (2016) 093B01, [arXiv:1606.07222](#) [hep-ph].
- [34] Y. Hosotani, “New Dimensions from Gauge-Higgs Unification,” [arXiv:1702.08161](#) [hep-ph].
- [35] Y. Hosotani and N. Yamatsu, “Electroweak Symmetry Breaking and Mass Spectra in Six-Dimensional Gauge-Higgs Grand Unification,” *Prog. Theor. Exp. Phys.* **2018** no. 2, (2018) 023B05, [arXiv:1710.04811](#) [hep-ph].
- [36] Y. Hosotani and N. Yamatsu, “Gauge-Higgs Seesaw Mechanism in 6-Dimensional Grand Unification,” *Prog. Theor. Exp. Phys.* **2017** no. 9, (2017) 091B01, [arXiv:1706.03503](#) [hep-ph].
- [37] C. Englert, D. J. Miller, and D. D. Smaranda, “Phenomenology of GUT-Inspired Gauge-Higgs Unification,” *Phys. Lett.* **B802** (2020) 135261, [arXiv:1911.05527](#) [hep-ph].
- [38] C. Englert, D. J. Miller, and D. D. Smaranda, “The Weinberg Angle and 5D RGE Effects in a SO(11) GUT Theory,” *Phys. Lett. B* **807** (2020) 135548, [arXiv:2003.05743](#) [hep-ph].
- [39] H. Georgi and S. L. Glashow, “Unity of All Elementary Particle Forces,” *Phys. Rev. Lett.* **32** (1974) 438–441.
- [40] K. Inoue, A. Kakuto, and Y. Nakano, “Unification of the Lepton-Quark World by the Gauge Group SU(6),” *Prog.Theor.Phys.* **58** (1977) 630.
- [41] H. Fritzsch and P. Minkowski, “Unified Interactions of Leptons and Hadrons,” *Ann. Phys.* **93** (1975) 193–266.
- [42] F. Gursev, P. Ramond, and P. Sikivie, “A Universal Gauge Theory Model Based on E_6 ,” *Phys. Lett.* **B60** (1976) 177.
- [43] R. Slansky, “Group Theory for Unified Model Building,” *Phys. Rept.* **79** (1981) 1–128.
- [44] N. Yamatsu, “Finite-Dimensional Lie Algebras and Their Representations for Unified Model Building,” [arXiv:1511.08771](#) [hep-ph].
- [45] Y. Kawamura, “Gauge Symmetry Breaking from Extra Space S^1/Z_2 ,” *Prog. Theor. Phys.* **103** (2000) 613–619, [arXiv:hep-ph/9902423](#) [hep-ph].
- [46] Y. Kawamura, “Split Multiplets, Coupling Unification and Extra Dimension,” *Prog. Theor. Phys.* **105** (2001) 691–696, [arXiv:hep-ph/0012352](#).
- [47] Y. Kawamura, “Triplet-Doublet Splitting, Proton Stability and Extra Dimension,” *Prog. Theor. Phys.* **105** (2001) 999–1006, [arXiv:hep-ph/0012125](#).

- [48] G. Burdman and Y. Nomura, “Unification of Higgs and Gauge Fields in Five-Dimensions,” Nucl. Phys. **B656** (2003) 3–22, [arXiv:hep-ph/0210257](#) [hep-ph].
- [49] C. S. Lim and N. Maru, “Towards a Realistic Grand Gauge-Higgs Unification,” Phys.Lett. **B653** (2007) 320–324, [arXiv:0706.1397](#) [hep-ph].
- [50] K. Kojima, K. Takenaga, and T. Yamashita, “Grand Gauge-Higgs Unification,” Phys. Rev. **D84** (2011) 051701, [arXiv:1103.1234](#) [hep-ph].
- [51] K. Kojima, K. Takenaga, and T. Yamashita, “Gauge Symmetry Breaking Patterns in an SU(5) Grand Gauge-Higgs Unification Model,” Phys. Rev. **D95** no. 1, (2017) 015021, [arXiv:1608.05496](#) [hep-ph].
- [52] N. Yamatsu, “Special Grand Unification,” Prog. Theor. Exp. Phys. **2017** no. 6, (2017) 061B01, [arXiv:1704.08827](#) [hep-ph].
- [53] N. Yamatsu, “String-Inspired Special Grand Unification,” Prog. Theor. Exp. Phys. **2017** no. 10, (2017) 101B01, [arXiv:1708.02078](#) [hep-ph].
- [54] N. Yamatsu, “Family Unification in Special Grand Unification,” Prog. Theor. Exp. Phys. **2018** no. 9, (2018) 091B01, [arXiv:1807.10855](#) [hep-ph].
- [55] N. Yamatsu, “ $USp(32)$ Special Grand Unification,” [arXiv:2007.08067](#) [hep-ph].
- [56] N. Maru and Y. Yatagai, “Fermion Mass Hierarchy in Grand Gauge-Higgs Unification,” PTEP **2019** no. 8, (2019) 083B03, [arXiv:1903.08359](#) [hep-ph].
- [57] B. Schrempp, F. Schrempp, N. Wermes, and D. Zeppenfeld, “Bounds on New Contact Interactions From Future e^+e^- Colliders,” Nucl. Phys. **B296** (1988) 1–25.
- [58] D. C. Kennedy, B. W. Lynn, C. J. C. Im, and R. G. Stuart, “Electroweak Cross-Sections and Asymmetries at the Z^0 ,” Nucl. Phys. **B321** (1989) 83–107.
- [59] SLD Collaboration, K. Abe et al., “Precise Measurement of the Left-Right Cross-Section Asymmetry in Z Boson Production by e^+e^- Collisions,” Phys. Rev. Lett. **73** (1994) 25–29, [arXiv:hep-ex/9404001](#) [hep-ex].
- [60] SLD Collaboration, K. Abe et al., “An Improved Measurement of the Left-Right Z^0 Cross-Section Asymmetry,” Phys. Rev. Lett. **78** (1997) 2075–2079, [arXiv:hep-ex/9611011](#) [hep-ex].
- [61] A. Blondel, B. W. Lynn, F. M. Renard, and C. Verzegnassi, “Precision Measurements of Final State Weak Coupling From Polarized Electron - Positron Annihilation,” Nucl. Phys. **B304** (1988) 438–450.
- [62] SLD Collaboration, K. Abe et al., “Measurement of A_b and A_c from the Left-Right Forward-Backward Asymmetry of Leptons in Hadronic Events at the Z^0 Resonance,” Phys. Rev. Lett. **74** (1995) 2895–2899.
- [63] SLD Collaboration, K. Abe et al., “Measurement of A_b from the Left-Right Forward-Backward Asymmetry of b Quark Production in Z^0 Decays Using a Momentum-Weighted Track-Charge Technique,” Phys. Rev. Lett. **74** (1995) 2890–2894.
- [64] SLD Collaboration, K. Abe et al., “Measurement of the Left-Right Forward-Backward Asymmetry for Charm Quarks with D^{*+} and D^+ Mesons,” Phys. Rev. Lett. **75** (1995) 3609–3613.
- [65] P. Langacker, “The Physics of Heavy Z' Gauge Bosons,” Rev. Mod. Phys. **81** (2009) 1199–1228, [arXiv:0801.1345](#) [hep-ph].

- [66] Y. Deguchi, H. Yamashiro, T. Suehara, T. Yoshioka, K. Fujii, and K. Kawagoe, “Study of Fermion Pair Events at the 250 GeV ILC,” in International Workshop on Future Linear Colliders. 2, 2019. [arXiv:1902.05245 \[hep-ex\]](#).
- [67] **LCC Physics Working Group** Collaboration, K. Fujii et al., “Tests of the Standard Model at the International Linear Collider,” [arXiv:1908.11299 \[hep-ex\]](#).
- [68] G. Moortgat-Pick et al., “The Role of Polarized Positrons and Electrons in Revealing Fundamental Interactions at the Linear Collider,” *Phys. Rept.* **460** (2008) 131–243, [arXiv:hep-ph/0507011 \[hep-ph\]](#).
- [69] T. Behnke, J. E. Brau, B. Foster, J. Fuster, M. Harrison, J. M. Paterson, M. Peskin, M. Stanitzki, N. Walker, and H. Yamamoto, “The International Linear Collider Technical Design Report - Volume 1: Executive Summary,” [arXiv:1306.6327 \[physics.acc-ph\]](#).
- [70] H. Baer, T. Barklow, K. Fujii, Y. Gao, A. Hoang, S. Kanemura, J. List, H. E. Logan, A. Nomerotski, M. Perelstein, et al., “The International Linear Collider Technical Design Report - Volume 2: Physics,” [arXiv:1306.6352 \[hep-ph\]](#).
- [71] C. Adolphsen, M. Barone, B. Barish, K. Buesser, P. Burrows, J. Carwardine, J. Clark, H. Mainaud Durand, G. Dugan, E. Elsen, et al., “The International Linear Collider Technical Design Report - Volume 3.I: Accelerator & in the Technical Design Phase,” [arXiv:1306.6353 \[physics.acc-ph\]](#).
- [72] C. Adolphsen, M. Barone, B. Barish, K. Buesser, P. Burrows, J. Carwardine, J. Clark, H. Mainaud Durand, G. Dugan, E. Elsen, et al., “The International Linear Collider Technical Design Report - Volume 3.II: Accelerator Baseline Design,” [arXiv:1306.6328 \[physics.acc-ph\]](#).
- [73] H. Abramowicz et al., “The International Linear Collider Technical Design Report - Volume 4: Detectors,” [arXiv:1306.6329 \[physics.ins-det\]](#).
- [74] **ALEPH** Collaboration, A. Collaboration, D. Collaboration, L. Collaboration, O. Collaboration, S. Collaboration, L. E. W. Group, S. E. Group, and S. H. F. Group, “Precision Electroweak Measurements on the Z Resonance,” *Phys. Rept.* **427** (2006) 257, [arXiv:hep-ex/0509008](#).
- [75] **Particle Data Group** Collaboration, M. Tanabashi et al., “Review of Particle Physics,” *Phys. Rev.* **D98** no. 3, (2018) 030001.
- [76] **SLD** Collaboration, K. Abe et al., “Polarized Bhabha Scattering a Precision Measurement of the Electron Neutral Current Couplings,” *Phys. Rev. Lett.* **74** (1995) 2880–2884, [arXiv:hep-ex/9410009 \[hep-ex\]](#).
- [77] **ALEPH, DELPHI, L3, OPAL, LEP Electroweak** Collaboration, S. Schael et al., “Electroweak Measurements in Electron-Positron Collisions at W-Boson-Pair Energies at LEP,” *Phys. Rept.* **532** (2013) 119–244, [arXiv:1302.3415 \[hep-ex\]](#).
- [78] D. Bardin, Y. Dydyshka, L. Kalinovskaya, L. Rumyantsev, A. Arbuzov, R. Sadykov, and S. Bondarenko, “One-Loop Electroweak Radiative Corrections to Polarized Bhabha Scattering,” *Phys. Rev.* **D98** no. 1, (2018) 013001, [arXiv:1801.00125 \[hep-ph\]](#).
- [79] V. I. Borodulin, R. N. Rogalyov, and S. R. Slabospitskii, “CORE 3.1 (COmpendium of RElations, Version 3.1),” [arXiv:1702.08246 \[hep-ph\]](#).